The Influence of Vesicle Size and Composition on α-Synuclein Structure and Stability

ARTICLE *in* BIOPHYSICAL JOURNAL · APRIL 2009

Impact Factor: 3.97 · DOI: 10.1016/j.bpj.2008.12.3940 · Source: PubMed

4 AUTHORS, INCLUDING:

Thomas Heimburg
University of Copenhagen
103 PUBLICATIONS **3,557** CITATIONS
SEE PROFILE

Daniel Otzen
Aarhus University
237 PUBLICATIONS **8,177** CITATIONS
SEE PROFILE

The Influence of Vesicle Size and Composition on α-Synuclein Structure and Stability

Lars Kjaer,[†] Lise Giehm,[†‡] Thomas Heimburg,[§] and Daniel Otzen[†‡*]
[†]Department of Life Sciences, Aalborg University, Aalborg, Denmark; [‡]Interdisciplinary Nanoscience Centre (iNANO), Aarhus University, Aarhus, Denmark; and [§]Niels Bohr Institute, University of Copenhagen, Copenhagen, Denmark

ABSTRACT Monomeric α-synuclein (αSN), which has no persistent structure in aqueous solution, is known to bind to anionic lipids with a resulting increase in α-helix structure. Here we show that at physiological pH and ionic strength, αSN incubated with different anionic lipid vesicles undergoes a marked increase in α-helical content at a temperature dictated either by the temperature of the lipid phase transition, or (in 1,2-DilauroylSN-Glycero-3-[Phospho-rac-(1-glycerol)] (DLPG), which is fluid down to 0°C) by an intrinsic cold denaturation that occurs around 10–20°C. This structure is subsequently lost in a thermal transition around 60°C. Remarkably, this phenomenon is only observed for vesicles >100 nm in diameter and is sensitive to lipid chain length, longer chain lengths, and larger vesicles giving more cooperative unfolding transitions and a greater degree of structure. For both vesicle size and chain length, a higher degree of compressibility or permeability in the lipid thermal transition region is associated with a higher degree of αSN folding. Furthermore, the degree of structural change is strongly reduced by an increase in ionic strength or a decrease in the amount of anionic lipid. A simple binding-and-folding model that includes the lipid phase transition, exclusive binding of αSN to the liquid disordered phase, the thermodynamics of unfolding, and the electrostatics of binding of αSN to lipids is able to reproduce the two thermal transitions as well as the effect of ionic strength and anionic lipid. Thus the nature of αSN's binding to phospholipid membranes is intimately tied to the lipids' physico-chemical properties.

INTRODUCTION

The 140-residue α-synuclein (αSN) protein is a central player in the etiology of Parkinson's disease. The protein, although natively unfolded in buffer as a monomer, aggregates to higher order structures in a series of events that ultimately leads to amyloid fibrils (1). An early stage oligomer appears to be implicated in cytotoxicity, as it is able to bind to anionic phospholipid membranes in vivo and induce uncontrolled permeabilization of small molecules such as Ca^{2+} ions (2–4). In vivo oligomers can also induce extracellular influx of Ca^{2+} and induction of apoptosis (5). The exact nature of the oligomer is still unresolved. Different incubation conditions lead to different types of oligomers with markedly different biological properties (5). Nevertheless, interactions with lipids are central to the protein's cytotoxicity and are most likely central to its as yet unidentified function(s). Endogenous αSN may regulate synaptic vesicle mobilization at nerve terminals (6). In yeast, genes involved in vesicle-mediated transport and lipid metabolism modify αSN toxicity (7); αSN overexpression in yeast interferes with ER-Golgi traffic and can be rescued by a protein (Rab1) involved in the same type of vesicle transport (8). Lipid binding and formation of α-helical structure inhibits fibril formation (9). The familial Parkinson's disease (PD) mutant A30P shows lower lipid affinity than wild-type αSN (10–13) and a concomitant reduction in α-helicity (14). This reduced binding affinity may be related to the mutant's inability to provide the same protective effect as wild-type αSN in mice lacking the CSP-α gene (15). Better insight into interactions between lipids and αSN monomers may also provide clues as to the protein's biological function.

Although cytoplasmic components may enhance αSN interactions with lipids and thus reduce the sensitivity of the interaction to changes in ionic strength (16), there is a large body of evidence supporting the direct interaction between αSN and lipids. As seen for many other flexible proteins, the fluctuating and dynamic nature of αSN (17) makes its structure highly sensitive to changes in pH, ionic strength, and charged amphiphiles. Thus, anionic lipid vesicles (11, 18–21), polyunsaturated fatty acids (22), and anionic detergents such as sodium dodecyl sulfate (18) induce α-helical structure in αSN, though it remains disputed whether the α-helicity observed in anionic vesicles is caused by a single unbroken helix (23,24) or by a bent helix leading to an antiparallel arrangement (25,26). Furthermore, fatty acids encourage the formation of soluble αSN oligomers in vivo (27,28). Binding of anionic amphiphiles is probably mediated by attractions to positively charged amino acids, given the preponderance of positive charges in the first 102 residues of αSN; in addition, fatty acid binding motifs have been suggested to occur in both termini (27). For anionic lipids, αSN shows preferential binding to smaller vesicles (25 nm diameter) rather than larger vesicles (125 nm diameter), probably because binding is facilitated by lipid packing defects (29). Interactions with anionic lipids predominantly occur at the interface in the liquid disordered phase according to electron paramagnetic resonance (EPR)-based temperature scans (30). This preference for the liquid disordered phase, corroborated by confocal laser scanning microscopy (13), no doubt reflects that the lipid interface has to be able to rearrange to accommodate the protein.

Submitted July 31, 2008, and accepted for publication December 30, 2008.

*Correspondence: dao@inano.dk

Editor: William C. Wimley.

0006-3495/09/04/2857/14 $2.00

doi: 10.1016/j.bpj.2008.12.3940

High concentrations of αSN (>30 μM) lyse and rearrange anionic membranes (3,31,32), probably because embedding in the upper part of the membrane (30,33,34) disrupts the membrane organization, analogous to antimicrobial peptides. However, there are numerous indications that αSN can interact with lipids in many different ways. αSN also binds to small zwitterionic vesicles in the gel phase but not liquid disordered phase (35), and αSN binding to small vesicles is encouraged by lipid phase separation induced by the presence of lipids of different chain lengths (19). This suggests a role for annealing defects in curved membranes and thus prevent premature fusion of synaptic vesicles (36). Interestingly, the presence of the zwitterionic phosphoethanolamine (in combination with anionic lipids) and a transmembrane potential induces ion channels with well-defined conductance states (37). All these observations suggest that many aspects of αSN-lipid interactions remain to be elucidated in detail.

Here we report an unusual ability of αSN to bind to large anionic vesicles and undergo reversible structural changes as a function of temperature. The structural changes show strong dependence on lipid/protein ratios, lipid-melting temperatures, ionic strength, lipid charge, and vesicle size. We have developed a thermodynamic model that captures many of these tendencies and shows that αSN interaction with lipids can be understood on the basis of simple mass action relations, coupled with cold and heat denaturation and lipid phase transitions. The model does not attempt to capture the reliance on a minimum vesicle size or the correlation between induced structure and chain length, but we suggest that these phenomena are qualitatively related to specific lipid properties in the phase transition region.

MATERIALS AND METHODS

αSN was expressed and purified as described (38). Protein concentration was determined using an extinction coefficient of 5120 M^{-1} cm^{-1}. 1,2-Dioleoyl-*sn*-Glycero-3-[Phospho-*rac*-(1-glycerol)] (DOPG); 1,2-Dioleoyl-*sn*-Glycero-3-Phosphocholine (DOPC); 1,2-Dilauroyl-*sn*-Glycero-3-[Phospho-*rac*-(1-glycerol)] (DLPG); 1,2-Dilauroyl-*sn*-Glycero-3-Phosphocholine (DLPC); 1,2-Dimyristoyl-*sn*-Glycero-3-[Phospho-*rac*-(1-glycerol)] (DMPG); 1,2-Dimyristoyl-*sn*-Glycero-3-Phosphocholine (DMPC); 1,2-Dimyristoyl-*sn*-Glycero-3-Phosphoethanolamine (DMPE); 1,2-Dipalmitoyl-*sn*-Glycero-3-[Phospho-*rac*-(1-glycerol)] (DPPG); and 1,2-Dipalmitoyl-*sn*-Glycero-3-Phosphocholine (DPPC) were from Avanti Polar Lipids (Alabaster, AL). All experiments were carried out in PBS buffer (10 mM sodium phosphate (pH 7.4) and 150 mM NaCl), unless otherwise stated. Single-component vesicles were suspended in buffer, subjected to five freezing-thawing cycles and extruded through filters of different pore sizes as described (39). For double-component vesicles, the lipids were first mixed in powder form, dissolved in chloroform, then dried and prepared as described above.

Circular dichroism spectra and thermal scans were performed on a Jasco J-810 spectrophotometer (Jasco Spectroscopic Co. Ltd., Hachioji City, Japan) using a 1-mm cuvette. Unless otherwise stated, both protein and lipid concentrations were 0.2 mg/mL (28 μM protein and 250–310 μM lipid, depending on the lipid used). Wavelength scans (250–190 nm) were recorded with a scan speed of 50 nm/min and five accumulations. Temperature scans were monitored at 215 nm with a scanning speed of 90°C/h in steps of 0.2 nm.

A note on reproducibility of thermal far-UV circular dichroism (CD) scans: For all lipids, the overall shape of the thermal scan is always retained from one experiment to the next, and the different transition temperatures vary by <1°C between triplicate measurements. We see some variation (~50%) in the slopes of the different plateau regions, whose ellipticity values vary by around 20% (data not shown). This variation is probably due to subtle changes in lipid vesicle size distributions that show natural variation from one preparation to the next. The variations are significantly smaller for experiments performed with the same vesicle batch.

Differential scanning experiments were performed on a VP-differential scanning calorimeter (MicroCal, Northampton, MA) using 1 mg/mL protein and 1 mg/mL lipid. A 0.7 mL sample and buffer reference were degassed in a vacuum chamber and thermal scans were done with low or no feedback, a scan rate of 60°C/h and a 0.16°C step size. Between runs, the calorimeter was cleaned by washing with 1% Mucasol, ethanol, and milliQ water for 10 min with each using a vacuum pump with the cleaning solution in the loop.

RESULTS AND DISCUSSION

αSN shows two characteristic thermal transitions in anionic lipids

When αSN is incubated with equal amounts (weight/weight) of 200-nm extruded vesicles of DMPG in the gel phase at 1°C, it retains the far-UV CD spectrum characteristic of a random coil (Fig. 1 *A*). However, as the temperature increases, the spectrum changes to that of a predominantly α-helical species, with two minima around 222 and 209 nm. The ellipticity (monitored midway between the two minima at 215 nm in Fig. 1 *B*) reaches its greatest value around 35°C (midpoint around 25°C), and then starts to decrease slowly in magnitude, rising steeply above 54°C to a new plateau from ~66°C onwards, with a midpoint around 61°C. All spectra between 1°C and 65°C show an isodichroic point around 203 nm, suggesting that both the downward transition and most of the upward transition represent a simple two-state transition from random coil to predominantly α-helical and back. Above 65°C, there is no longer any isodichroic point, suggesting that we are monitoring another structural change at this stage. Consistent with this observation, all of the transitions are completely reversible if the temperature does not exceed 60–65°C (the end of the second major transition), as repeated upward and downward cycles, as well as scans carried out at scan rates between 10°C and 90°C, lead to superimposable scans (data not shown). There is essentially no change if we ''jump in'' by preincubating at a certain temperature (e.g., the plateau between the two transitions) and then proceed with a temperature rise. Thus the system immediately adjusts to the temperature in question, in good accord with the complete reversibility of the process up to 65°C. At higher temperatures we cannot exclude the formation of covalent modifications or irreversible aggregation (see below). Similar isodichroic points at 203 nm up to ~65°C are seen for DLPG and DPPG (data not shown).

αSN undergoes the same type of transition in the anionic lipids DLPG and DPPG (Fig. 1 *B*), although the downward transition is shifted to higher temperatures in DPPG (midpoint around 40°C) and to lower temperatures in DLPG (midpoint around 10°C). For DLPG, DMPG, and DPPG, the midpoint corresponds reasonably to the phase

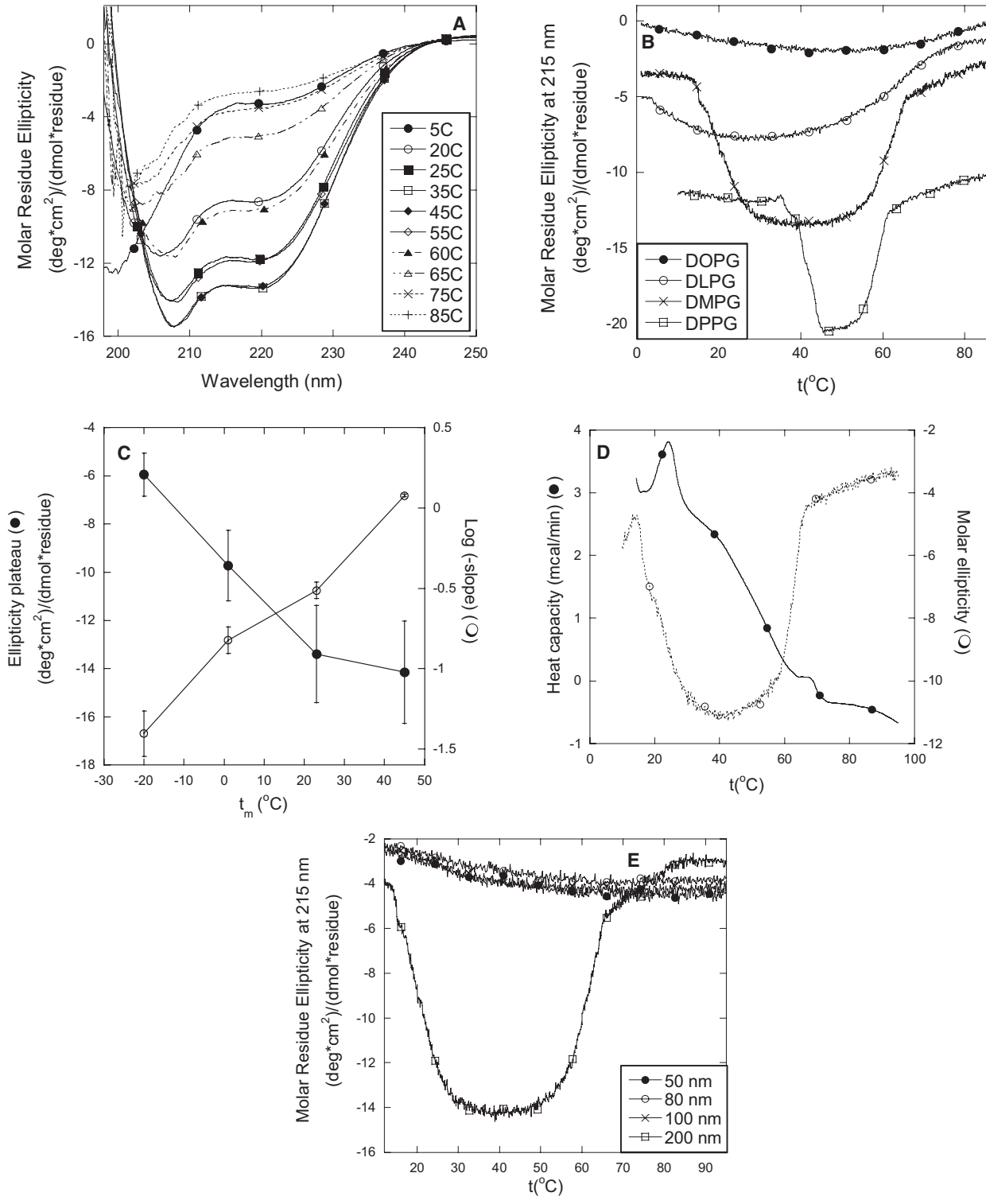

FIGURE 1 (*A*) Thermal far-UV CD scans of 0.2 mg/mL αSN in 0.2 mg/mL 200-nm DMPG vesicles as a function of increasing temperature. (*B*) Thermal far-UV CD scans at 215 nm for 0.2 mg/mL αSN in 0.2 mg/mL 200-nm vesicles of different lipids. For clarity, data have been offset for three lipids by the following number of units: DOPG + 4, DLPG + 2, and DPPG − 6. (*C*) Linear correlation between melting temperature t_m of the lipids and the molar ellipticity of the plateau following this transition (*solid circles*). A linear correlation is also seen between t_m and the log of the slope of this transition (*open circles*). Error bars represent estimates of 20% errors from plateau scans and 10% from slopes from triplicate experiments. (*D*) Differential scanning calorimetry scan of αSN in DMPG (*solid line*) contrasted with the corresponding far-UV CD scan (*stippled line*) from (*B*). DSC scans were with 1 mg/mL αSN in 1 mg/mL lipid whereas CD scans were with 0.2 mg/mL αSN in 0.2 mg/mL lipid. (*E*) Thermal far-UV CD scans of 0.2 mg/mL αSN in 0.2 mg/mL DMPG as a function of extruded vesicle size. Notice the complete disappearance of distinct thermal transitions for vesicles with diameters below 200 nm.

change at temperature t_m where the lipid goes from the gel phase (below t_m) to the liquid disordered phase (above t_m). However, the steepness of this transition markedly increases from DLPG and DOPG as we go to DMPG and DPPG. Similarly, the upward transition is much steeper in DMPG (steep curve from 57°C to 67°C) and DPPG (steep curve from 55°C to 61°C) than in DLPG (steep curve from 52°C to 72°C), indicating that the cooperativity of the transition increases with increasing lipid transition temperature t_m. In the 18-carbon unsaturated lipid DOPG, by contrast, both transitions are smoothed out and hardly visible (Fig. 1 *B*). The degree of α-helicity attained by αSN at the end of the downward transition correlates linearly with t_m (Fig. 1 *C*). The same insert also illustrates a linear correlation between the slope of the downward transition and t_m. Similar types of correlation exist between t_m and the slope and plateau level associated with the upward transition (data not shown).

Both transitions in DMPG are also seen as classical enthalpic peaks by differential scanning calorimetry (DSC) (Fig. 1 *D*). There is a slight shift in the second transition, which peaks around 68°C, around 6°C higher than that in CD, but this can be attributed to the somewhat higher lipid concentrations required for DSC measurements (1 mg/mL) versus CD (0.2 mg/mL).

Importantly, these two transitions are very sensitive to vesicle size. In the great majority of our experiments, they are not observed in far-UV CD thermal scans for DMPG vesicles smaller than around 200 nm (Fig. 1 *E*). If vesicles smaller than 200 nm are cooled down below the t_m, they coalesce to larger structures that are able to induce structure in αSN upon subsequent heating (data not shown). Higher concentrations (1 mg/mL and above) of 100-nm vesicles led to more distinct transitions that gradually approached those of the 200-nm vesicles in terms of ellipticity values, indicating a difference in affinity between the two classes of vesicles (data not shown). However, nonextruded vesicles (which have sizes from several hundred nm up to a few μm) show the same behavior as 200-nm vesicles (data not shown).

The thermal transitions are not artifacts of lipid networks but represent genuine protein conformational changes

We suspected that these transitions might be artifacts of lipid reorganization rather than protein structural changes. At low salt concentrations, anionic lipids are known to form extensive bilayer networks (40), which could lead to light-scattering artifacts. However, this effect is effectively screened by increasing salt and effectively disappears around physiological salt concentrations, such as those used in our study (150 mM NaCl). In addition, we have accumulated several other observations that argue against a simple lipid-based artifact rather than a genuine induction of structure.

First, the transitions are not seen when lipids are incubated in the absence of protein (data not shown) or even in the presence of a membrane-interacting protein such as the antimicrobial peptide Novispirin, which is known to have a preference for anionic lipids (39) (Fig. 2 *A*). They do not occur when αSN is heated in the absence of lipid (Fig. 2 *A*). Dynamic light-scattering experiments do not indicate significant vesicle changes over the measured temperature range (data not shown). In addition, in mixtures of DOPG with DMPG or DLPG, where the lipid thermal transitions are altered, the observed transitions correspond to those seen in neat DMPG or DLPG (see below). Second, and in even greater contrast to the lipid network transition (40), the αSN transitions in DMPG also occur well above 150 mM NaCl (Fig. 2 *B*), although the amount of structure induced by the first transition decreases markedly with increasing salt concentration, suggesting that the interactions with DMPG are mediated by electrostatic interactions. The midpoints of both the low- and high-temperature transitions, as well as the plateau levels between the transitions, scale linearly with the square root of the ionic strength, which is a measure of the solution's screening ability (Fig. 2 *C*). The shift in midpoint is much more pronounced for the high-temperature transition. The two transitions converge toward each other and merge around 600 mM NaCl.

Third, and probably most importantly, we see significant differences compared to wild-type αSN when we measure thermal far-UV CD scans using two naturally occurring mutant variants of αSN, namely A30P and A53T (Fig. 2 *D*), which differ in their lipid binding affinities (12) and their amount of residual structure compared to wild-type (14). All three proteins show the same low-temperature transition around 20°C (governed by the lipid transition, see below), but there is a marked variation in the high-temperature transition. A30P, which shows decreased affinity for membranes compared to wild-type (10), shows a midpoint around 50°C, whereas A53T has a midpoint around 57°C. Both transition temperatures are significantly lower than the 62°C shown by wild-type. It is reasonable to expect that the altered membrane binding properties of the αSN mutant A30P and the reported disruption of both mutants' structure compared to wild-type αSN (with concomitant reduced stability) will affect these thermal transitions.

Fourth, we have also analyzed the dependence of this transition on the amount of lipid present (Fig. 3 *A*). The ellipticity plateau between the two transitions increases with lipid concentration up to around 0.5 mg/mL (i.e., 2.5 lipid/αSN w/w) after which it remains constant (Fig. 3 *B*), indicating saturation of binding. The data agree reasonably with the approximate 1.7 DMPG/αSN(w/w) binding ratio observed by EPR (30). With increasing lipid concentration, the low- and high-temperature transitions shift symmetrically away from each other, respectively decreasing and increasing by around 6–8°C between 0.1 and 5 mg/mL lipid.

Finally, if we keep lipid concentration constant at 0.2 mg/mL and vary protein concentration 20-fold between 0.05 and 1.0 mg/mL, we obtain the same two transitions in all cases,

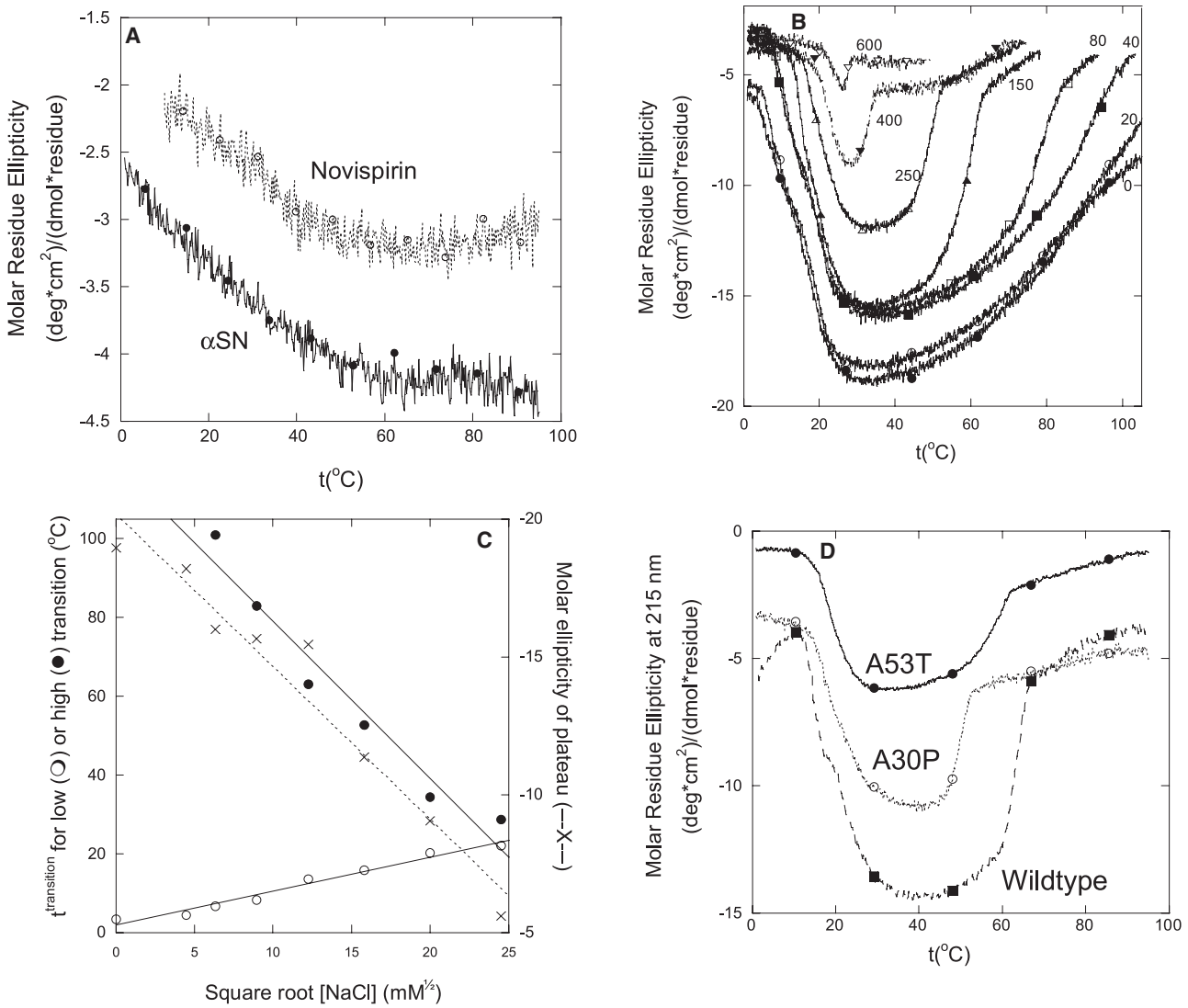

FIGURE 2 (*A*) Thermal far-UV CD scans of 0.2 mg/mL αSN in the absence of lipid and 0.2 mg/mL of the antimicrobial peptide Novispirin in 0.2 mg/mL 200 nm DMPG vesicles. (*B*) Thermal far-UV CD scans of 0.2 mg/mL αSN in 0.2 mg/mL 200-nm vesicles of DMPG in 10 mM sodium phosphate pH 7.4 and 0–600 mM NaCl (NaCl concentrations indicated in mM in the graph). (*C*) Transition temperatures for the first and second thermal transitions from (*B*), as well as the molar ellipticity at 215 nm (in units of (deg cm^2)/(dmol residue)) of the plateau level between the two transitions, plotted versus the square of the ionic strength. Solid lines are best linear fits to the two transition temperature plots, whereas the stippled line is the best fit to the plateau plot. To minimize ambiguity, we estimated the two sets of transition temperatures as follows: for the first transition, the temperature at which the transition starts (determined as the intersection between the preceding baseline and the first transition slope); for the second transition, the temperature at which the transition stops (determined as the intersection between the second transition slope and the subsequent baseline). (*D*) Thermal far-UV CD scans of wild-type αSN and the two mutants A30P and A53T in 0.2 mg/mL 200-nm DMPG vesicles. Protein concentration 0.2 mg/mL.

although the low protein concentration at 0.05 mg/mL gives a very small signal change and a broadening of the transition (Fig. 3 *C*). The low-temperature transition occurs around 18°C in all three cases, but there is a systematic shift upwards in the high-temperature transition, which may be related to stabilization of αSN by oligomerization (see below).

All these experiments illustrate that by using 0.2 mg/mL lipid with 0.2 mg/mL protein, the αSN is in fact nicely placed in the steepest part of a binding transition, so that even small changes in the binding affinity (due to changes in the lipid headgroup, chain length, ionic strength, etc.) are translated into large changes in the degree of folding. Importantly, these observations strongly indicate that protein properties rather than lipid artifacts dictate these transitions.

Anionic lipid is crucial for αSN binding

We also find that the amount of anionic lipid plays an important role. In thermal scans of αSN in mixed vesicles with increasing concentrations of DMPC and decreasing concentrations of DMPG, the high-temperature transition decreases drastically to a midpoint around 34°C in 80% DMPG and 28°C in 60%

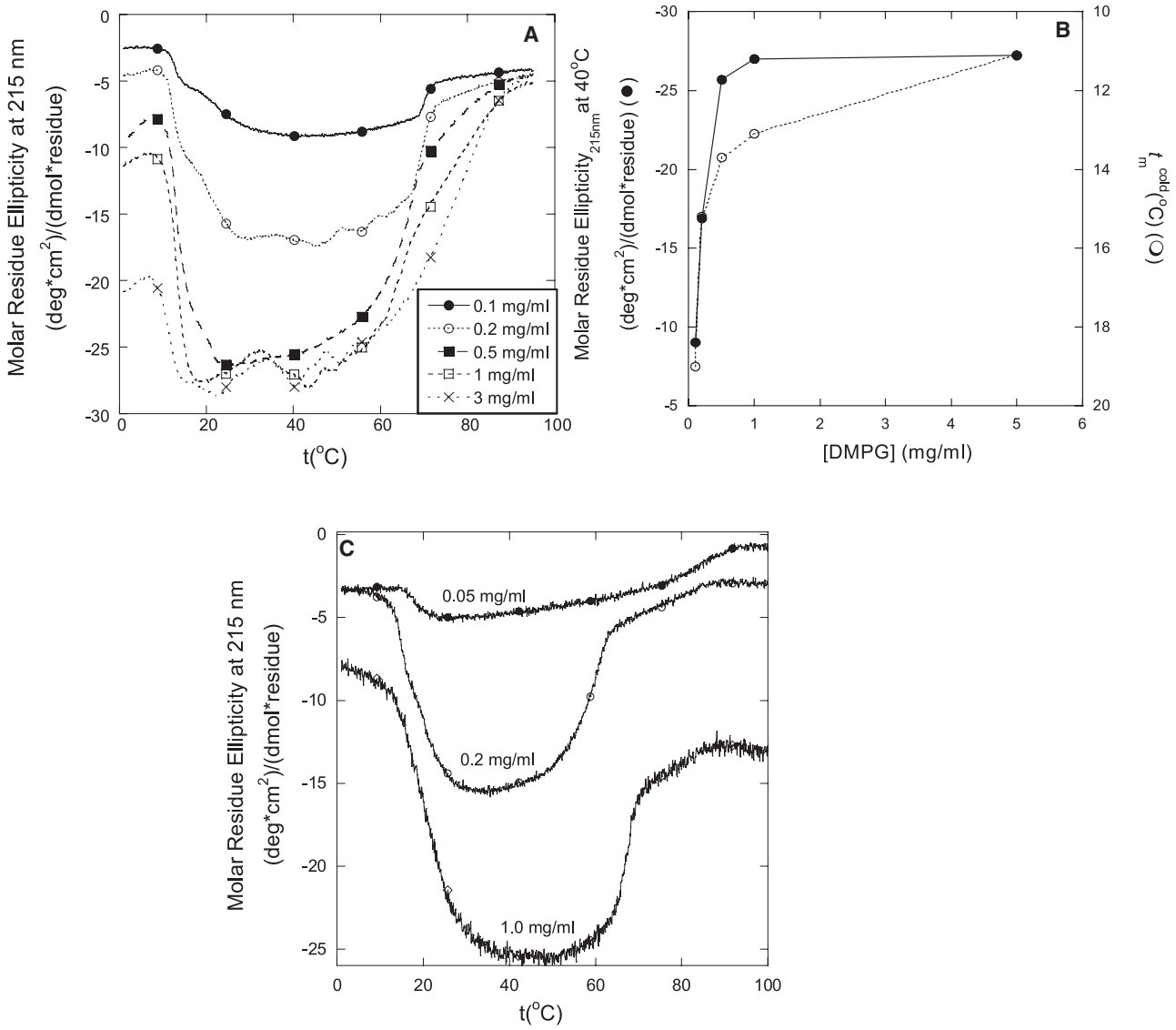

FIGURE 3 (*A*) Thermal far-UV CD scans of 0.2 mg/mL αSN in different concentrations of 200-nm DMPG vesicles. (*B*) Ellipticity at 215 nm of the scans in (*A*) versus lipid concentration (*solid circles*) and midpoint of thermal transition (*open circles*), determined as the temperature at which ellipticity is half-way between the preceding baseline level and the plateau level reached at the end of the transition. (*C*) Thermal far-UV CD scans of different concentrations of αSN in 0.2 mg/mL 200-nm DMPG vesicles.

DMPG, whereas the low-temperature transition remains reasonably constant around 20°C (Fig. 4 *A*). Thus the plateau region between the two transitions shrinks and finally disappears entirely at 40% DMPG and below, leading to a complete absence of transition. Interestingly, when we replace DMPG with the nonbilayer-forming lipid DMPE instead of DMPC, the midpoint of the high-temperature transition is not lowered so markedly as in DMPC, although the overall level of structure induction (the plateau after the low-temperature transition) is reduced just as much as in DMPC (Fig. 4 *B*). A similar reduction in structure induction and lowering of the high-temperature transition has been reported in mixed vesicles of DOPC, DOPG, and 1,2-Dioleoyl-*sn*-Glycero-3-Phosphoethanolamine (DOPE) (37). Thus different zwitterionic headgroups appear to induce subtle changes in the types of interactions between αSN and vesicles, in good accordance with the suggestion that αSN is embedded in the upper part of the membrane (34), and therefore the degree of binding of αSN, and its consequent stabilization against unfolding, is sensitive to the nature of the headgroup. However, changes in lipid charge by addition of phosphocholine (PC) lipids shift the plateau midpoint to lower temperatures (Fig. 4 *A*), because the high-temperature transition is shifted down more than the low-temperature transition. The shift is less pronounced if we use phosphoethanolamine (PE) instead of PC lipids (Fig. 4 *B*) and there are also subtle changes in the thermal profile (compare 80% DOPG-20% DOPC in Fig. 4 *A* with 80% DOPG-20% DOPE in Fig. 4 *B*). Thus PE affects αSN

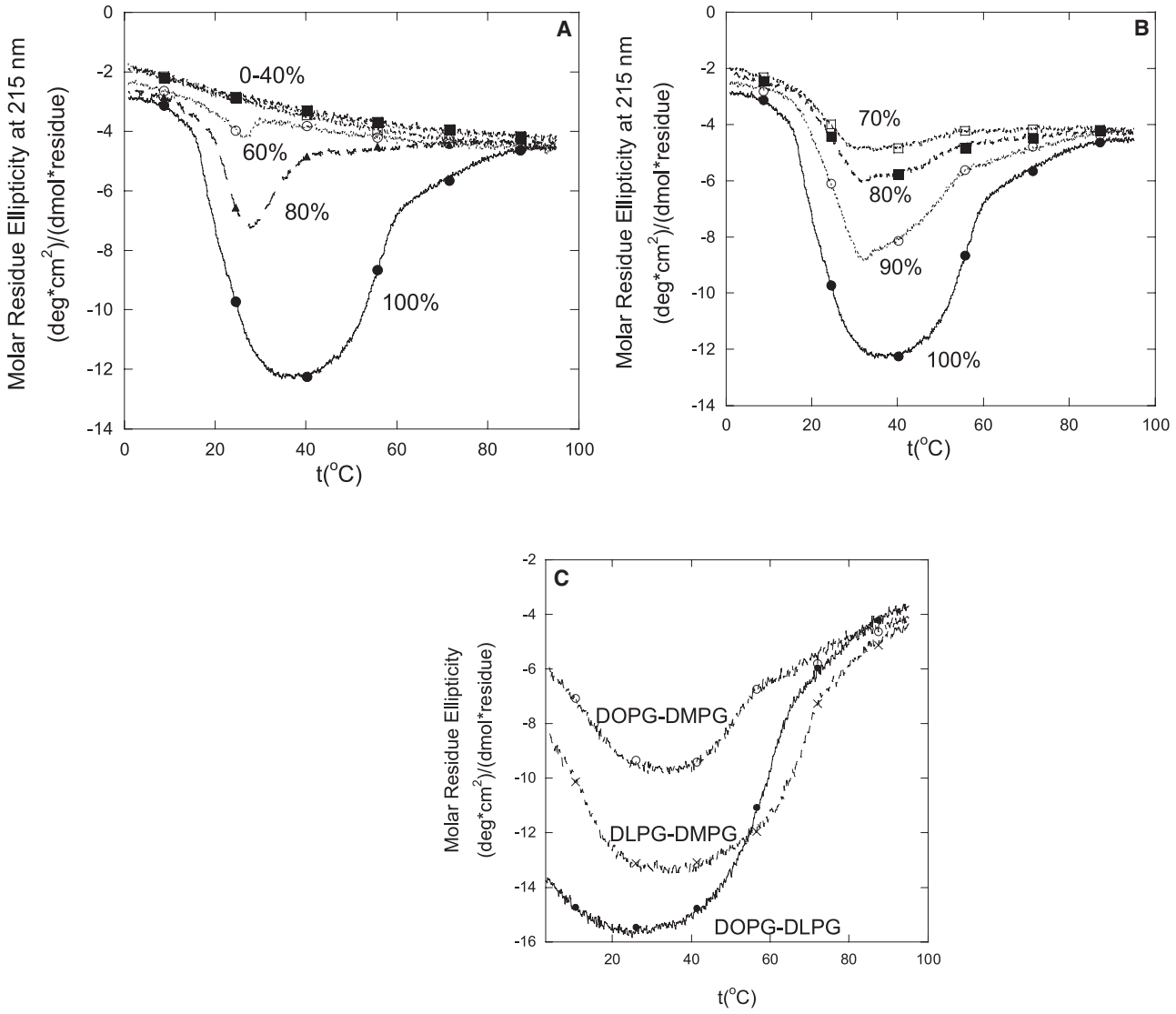

FIGURE 4 Thermal far-UV CD scans of 0.2 mg/mL αSN in 0.2 mg/mL 200-nm vesicles of mixtures of DMPG and (*A*) DMPC or (*B*) DMPE. The percentages indicate the fraction of DMPG (w/w) in the lipid mixture. (*C*) Thermal far-UV CD scans of 0.2 mg/mL αSN in 0.2 mg/mL 200-nm vesicles of 1:1 mixtures of different lipids.

differently from PC in anionic lipids, consistent with the specific role of PE lipids together with anionic lipids in forming ion channels with well-defined conductance states in the presence of a transmembrane potential (37). The strongly reduced binding of αSN to large vesicles in the liquid disordered phase in the presence of PC presents a symmetric contrast to αSN's preference for small zwitterionic vesicles in the gel phase but not liquid disordered phase (35). It clearly illustrates that there are numerous combinations of vesicle size, state, and charge that encourage αSN binding, revealing a complex energy landscape for protein-lipid interactions.

Given that αSN binding to small vesicles is encouraged by lipid phase separation induced by the presence of lipids of different chain lengths (19), we explored the effect of different mixed vesicles. Although there are no clear thermal transitions in neat DOPG (Fig. 1 *B*), the combination DOPG-DMPG leads to two clear transitions (Fig. 4 *C*), of which the first transition is shifted around 6°C downwards (to around 13–16°C) compared to neat DMPG. Binary lipid mixtures will typically show broad melting profiles containing peaks with individual peaks that do not coincide with those of the pure components, but are shifted closer to each other (41). In a DOPG-DMPG or DLPG-DMPG mixture, we would therefore expect a major melting peak 6–8°C below that of DMPG (t_m 23°C), i.e., around 15°C in good accordance with the observed transitions. The DOPG-DLPG mixture, on the other hand, remains liquid disordered throughout the scanned region and the transition temperature is accordingly not affected compared to pure DLPG.

A simple model to rationalize αSN behavior in vesicles

To develop a framework that may qualitatively reproduce at least some of the phenomena observed here, we develop a simple model for αSN interactions with vesicles. Let us consider the following simple binding scheme:

$$NL \overset{K_1}{\longleftrightarrow} DL \overset{K_2}{\longleftrightarrow} D + L,$$

where L is lipid and NL and DL are the native (i.e., α-helix rich) and denatured (intrinsically unstructured) protein, respectively, embedded into the membrane. This scheme can be further simplified by assuming that the surface adsorbed denatured state does not exist, due to the high energetic cost of burying unpaired hydrogen bond acceptors and donors (found in D to a much greater extent than N) in an amphiphilic environment (42):

$$NL \overset{K}{\longleftrightarrow} D + L.$$

We assume that αSN molecules bind independently and noncooperatively (as indicated by the hyperbolic binding curve in Fig. 3 *B*).

From this we derive the following relationship:

$$\begin{aligned}\frac{[D]}{[NL]} &= \frac{c_o}{[L]}\exp\left(-\frac{\Delta G}{RT}\right)\\ &= \exp\left(-\frac{\Delta G + RT\ln([L]/c_o)}{RT}\right)\\ &= \exp\left(-\frac{\Delta G + \Delta G_{\text{conc}}}{RT}\right),\end{aligned} \tag{1}$$

where c_o =1 mol/L is the standard state concentrations and $\Delta G = \Delta G_{\text{unfolding}} + \Delta G_{\text{hydrophobic}} + \Delta G_{\text{electrostatic}} + \Delta G_{\text{lipid}}$. The first two terms in this equation may be described by standard enthalpy and entropy terms according to Privalov (43), whereas the third electrostatic term is treated according to Heimburg and Marsh (44), and the fourth term is an entropic term related to lipid concentration. This leads to the following total equation:

$$\begin{aligned}\Delta G_{\text{tot}} &= \Delta H_o + \Delta c_p(T - T_m) - T\left(\frac{\Delta H_o}{T_m} + \Delta c_p \ln\frac{T}{T_m}\right)\\ &\quad + 2Z \cdot RT\ln\left(K_o\frac{\sigma}{\sqrt{I}}\right) + RT\ln([L]/c_o),\end{aligned} \tag{2}$$

where ΔH_o is the enthalpy of unfolding, Δc_p the heat capacity difference between the folded and the unfolded state (which we assume to be constant with temperature for simplicity), T_m the unfolding temperature, Z is the effective charge of the protein seen by the surface (assumed to be +4 for αSN by disregarding the C-terminal 45 residues that form an acidic tail assumed to be away from the membrane (18)), σ is the charge density of the surface (for DMPG it is about one charge (1.602×10^{-19} C) per 50 Å^2, i.e., $\sigma = 0.320$), I is the ionic strength, and K_o is an intrinsic constant whose size depends on the magnitude of the hydrophobic and other nonelectrostatic contributions to binding. The strong linear correlations between salt concentration and the transition temperatures as well as plateau levels (Fig. 2 *C*) support the inclusion of a term for ionic strength.

When $\Delta G_{\text{tot}} < 0$, the protein is unfolded, when $\Delta G_{\text{tot}} > 0$ it is folded. The unfolding temperatures are found for $\Delta G_{\text{tot}} = 0$. Depending on the parameters in Eq. 2, one can get zero, one, or two unfolding temperatures, representing cold denaturation and hot denaturation, respectively. Cold denaturation occurs upon lowering the temperature rather than raising it; for simplicity we shall also refer to this process as cold denaturation irrespective of the direction of the temperature change. Cold denaturation arises from a positive value for Δc_p, arising from the strong temperature dependence of the interaction of water with apolar residues of the peptide chain, which makes the exposure of apolar amino acids to water favorable at low temperatures, thus triggering unfolding upon cooling (45).

An additional factor needs to be taken into account. The lipid phase transition appears to play an important role for αSN's ability to bind membranes, given that the low-temperature transition coincides with t_m (Fig. 1 *B*), and supported by the fact that the high-temperature transitions are affected much more than the low-temperature transition by changes in ionic strength, anionic lipid fraction, and lipid concentration. The phase transition can easily be taken into account by assuming that αSN only binds to the liquid disordered phase, in good agreement with previous reports (13,30). We can calculate the amount of fluid lipid as a function of temperature as follows. For a lipid with melting point T_m, enthalpy of melting ΔH_{Tm} and cooperative unit size, n, the equilibrium constant between fluid and gel membrane is (41):

$$K = \exp\left(-n^*\Delta H_{T_m}\left(1 - \frac{T}{T_m}\right)/RT\right). \tag{3}$$

The cooperative unit size describes how many lipids melt simultaneously in a cluster or a domain and thus how narrow the transition is. Typical values are $n = 100$ for unilamellar systems and $n = 1000$ for multilamellar systems. In addition, we also consider the term α, which is the number of lipids bound to each αSN molecule (which we estimate to be eight on the basis of the saturation level at 2.5 lipid/αSN w/w in Fig. 3 *B*). Thus in Eqs. 1 and 2, the lipid concentration $[L]$ can be replaced by the concentration of binding sites in the fluid state, i.e., $([L]/\alpha) \times K/(1 + K)$.

The equation successfully predicts most of our experimental observations

To implement this equation, we use the following standard values for the key parameters:

$\Delta H_o = 150$ kJ/mol (lower than the 250 kJ/mol for e.g., the membrane-binding protein cytochrome *c* (41) to reflect that αSN is probably only partially folded in the membrane), $T_m^{\alpha SN} = 330$ K (corresponding to the observed second thermal transition around 57°C), $\Delta c_p = 6$ kJ/mol/K (midway between those of the two proteins cytochrome *c* (41) and myoglobin (43), to reflect that αSN's molecular weight is midway between the two), $K_o^{el} = 0.1$ mol/L, $Z = +4$ and known values of ΔH_{Tm} and t_m for the different lipids (see legend to Fig. 5 *A*) Using these values, we can predict how the thermal denaturation profile varies as a function of lipid composition, ionic strength, and lipid concentration. The values of these parameters are not fixed but are used to illustrate the predictive powers of our equation.

As seen in Fig. 5 *A*, the positions of the two thermal transitions correspond very well to the experimental data for DPPG, DMPG, and DLPG, but not for DOPG (see below). The slope of the first thermal transition (which reflects the value of ΔH_{Tm}) increases with t_m and thus chain length. This increase is also observed when comparing the transition in DMPG versus DPPG (Fig. 1 *B*).

Note that for DLPG (T_m −2°C), we still observe a low-temperature transition around 10–15°C although the lipid remains fluid throughout the measured temperature range. DLPG thus illustrates that we can observe cold denaturation of αSN at low lipid concentrations provided denaturation occurs at temperatures above the lipid phase transition. Interestingly, the same 10–15°C transition is observed when we use vesicles composed of 1:1 mixtures of DOPG-DLPG, DOPG-DMPG, and DMPG-DLPG (Fig. 4 *C*). In the temperature range between the melting points of the two lipid components, these lipid mixtures will consist of two coexisting phases, namely a liquid disordered phase consisting mainly of the lipid with the lower melting temperature and a gel phase with mainly the higher-melting lipid. Thus αSN will undergo cold denaturation in these mixtures provided there is some fluid phase present. Note that neat DOPG is an anomaly, as the two experimentally observed transitions in DOPG are very shallow and thus difficult to assign to any specific structural transition. The maximum amount of structure attained in DOPG is much lower than that of the other lipids although DOPG remains in the liquid disordered phase throughout the tested temperature range (see further discussion below).

In our model, there is good correspondence between model and data in the second transition, which shifts experimentally by around 6–8°C and 10–12°C in the model. For the first transition, increasing DMPG concentration leads to a downward shift in t_m from 23.7°C to 23.0°C (Fig. 5 *B*) and a resulting shift in the first transition by the same amount (Fig. 5 *C*). This shift is however much more modest than the experimentally observed decrease in the first transition temperature from around 20°C to around 12°C (Fig. 3 *B*). If proteins only partition into the liquid disordered phase, this will lead to freezing point depression (46,47). Such a phenomenon will mainly occur at low lipid/protein ratios, in contrast to the observed trend. However, if we assume that αSN can bind with equal affinity to both gel phase and liquid disordered phase, we get a much more pronounced shift in the low-temperature transition (data not shown). This suggests that αSN in fact has a weak affinity for the lipid gel phase that allows it to bind and undergo structural changes, provided sufficient lipid is present (41).

Electrostatics play a large role in the αSN-lipid interactions. The effect of ionic strength, described in Eq. 2 is to shift the first transition down by around 5°C and the second transition up by around 50°C (Fig. 6 *A*), in remarkably good agreement with data (Fig. 2 *B*). It is also possible to take the lipid charge density into account in our model. If proteins bind to a mixed lipid membrane (made of charged and uncharged lipid), the charge density is lower and therefore the binding is weaker. If the lipids mix ideally, then the binding of the protein may lead to an accumulation of the charged lipid underneath the protein. Under these conditions the intrinsic binding constant K_o in Eq. 2 has to be replaced by a term that contains the fraction of charged lipid, f_A, the relative association constant, K_r, of the charged lipid to the protein (as compared to the uncharged lipid), and the area occupied by a protein molecule on the membrane surface relative to that of a single lipid molecule, α. As described in detail elsewhere (48), this leads to the following term:

$$K_0 \rightarrow K_o \frac{f_A^{2Z}(1 - f_A + f_A K_r)^{\alpha}}{K_r^{f_A \alpha}}. \quad (4)$$

With standard values ($\alpha = 8$ and $K_r = 4.8$) used for cytochrome binding to lipid membranes (44,48), we observe (Fig. 6 *B*) that as the fraction of charged lipid decreases, so there is a reduction in the degree of folding in the intermediate regime between the two transitions. At a charge fraction $f_A = 0.6$, folding has practically disappeared. As seen for changes in ionic strength, the high-temperature transition is affected much more strongly than the low-temperature transition.

Thermal scans at different αSN concentrations (Fig. 3 *C*) reveal that the high-temperature transition is shifted upwards at higher protein concentrations. This indicates that association or aggregation of αSN on the membrane stabilizes the protein against thermal unfolding, which is in good agreement with previous reports that membranes stimulate αSN aggregation (20,49). For simplicity, we have not included this aspect in our model. The oligomerization may be modeled in numerous ways and may in fact lead to a continuum of different species, about which our limited data cannot provide more detailed information. More systematic future studies may shed further light on this.

Observations not addressed by the model

Thus our simple model captures most of our data. However, two aspects have not been addressed:

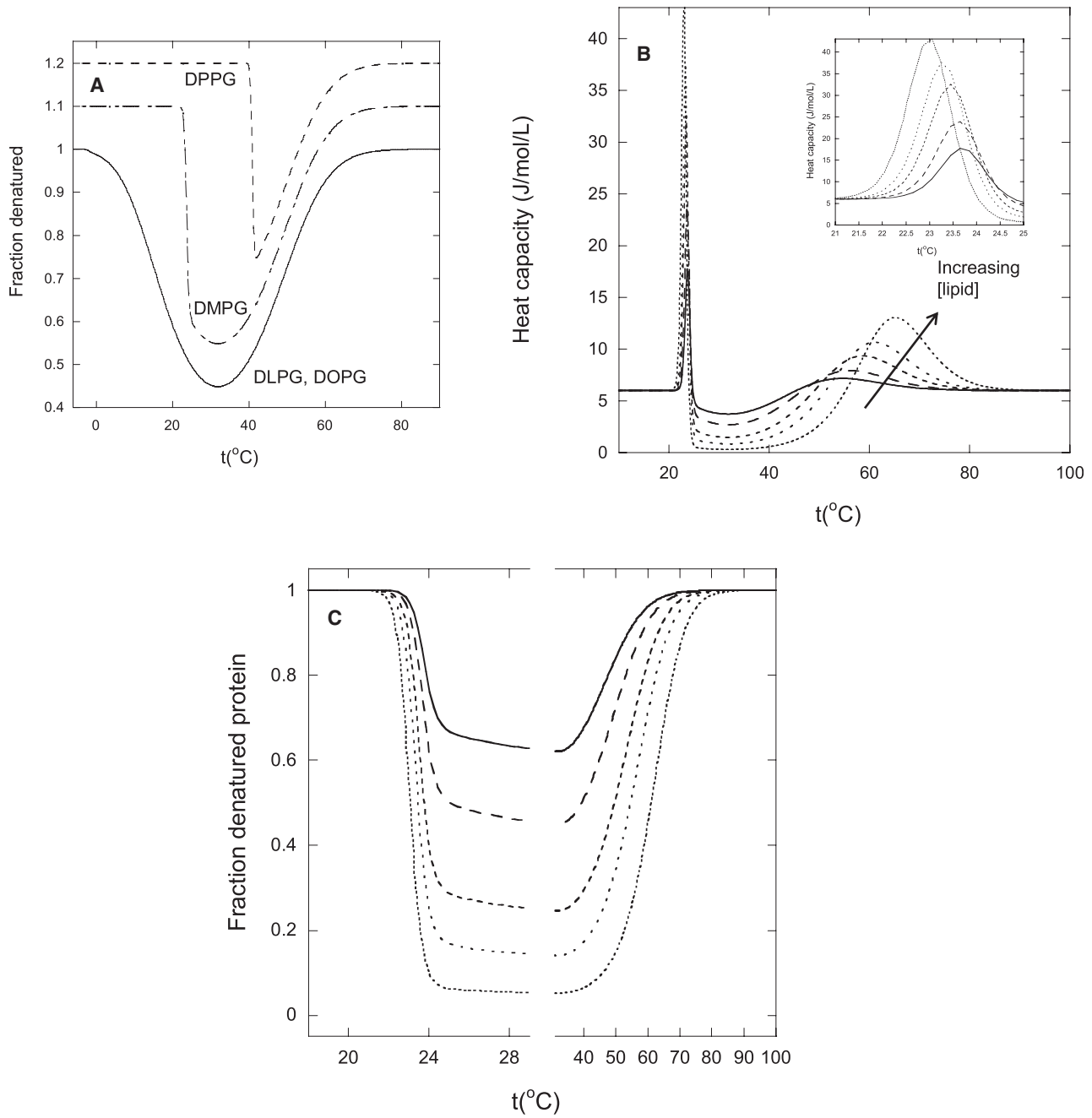

FIGURE 5 Predicted behavior of αSN when heated in the presence of different concentrations of anionic lipid, based on Eq. 2 (including lipid thermal transitions). (*A*) Thermal transitions in different lipids, depicted as the fraction unfolded protein as a function of temperature (0.2 mg/mL protein and 0.2 mg/mL lipid in 160 mM ionic strength). The following melting enthalpies ΔH_{Tm} and melting temperatures t_m were used: DPPG: $\Delta H = 35$ kJ/mol, $t_m = 41.2°C$; DMPG: $\Delta H = 24$ kJ/mol, $t_m = 24°C$; DLPG: $\Delta H = 13$ kJ/mol, $t_m = -2°C$. For DOPG ($t_m = -20°C$), the lipid was considered fluid in the whole temperature range. The unit of cooperativity n was set to 100, which is typical of unilamellar systems such as those used here. Values for DMPG and DPPG have been offset by 0.1 and 0.2 units on the y axis for clarity. Values for DOPG and DLPG are identical given that they are both fluid in the temperature range where αSN undergoes cold denaturation (>0°C). (*B*) Heat capacity changes and (*C*) corresponding degree of folding of αSN (0.2 mg/mL protein and 160 mM ionic strength) as a function of DMPG concentration. The heat capacity changes contain contributions both from the DMPG phase transition (highlighted in the insert to (*B*)) and from αSN folding/unfolding.

Different degrees of structure induced in different lipids

It is clear from Fig. 1 *B* (and insert) that the higher the lipid-melting temperature, the higher the proportion of αSN that is folded (measured as the ellipticity plateau level between the two thermal transitions). Based on the titration in Fig. 3, we can estimate that only up to 50% of αSN is bound to lipid in Fig. 1 *B*. Thus under these conditions we are in the middle of the binding transition, making binding very sensitive to

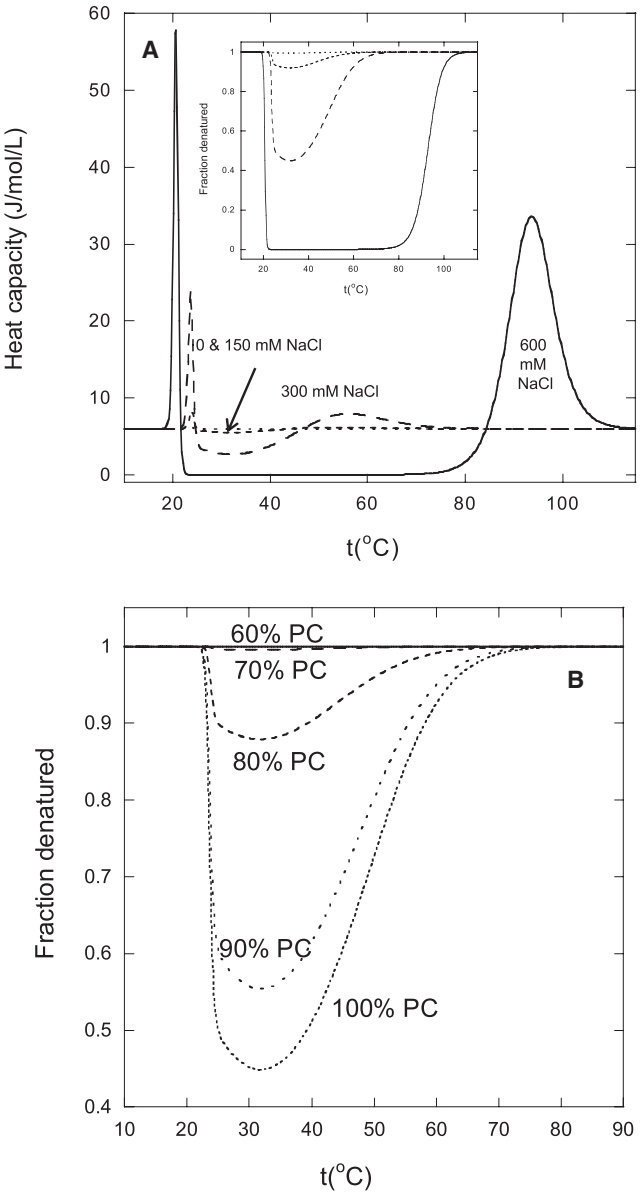

FIGURE 6 (*A*) Predicted effect of different ionic strength on the temperature-dependent folding of 0.2 mg/mL αSN in 0.2 mg/mL DMPG. Insert shows the change in the degree of folding of αSN as a function of temperature. (*B*) Predicted effect of the reduction in the fraction of anionic lipid (w/w) on the αSN thermal transitions.

different lipid properties. Given that the concentration of the different lipids in Fig. 1 *B* is the same (0.2 mg/mL) in all cases, we conclude that αSN has higher affinity for the liquid disordered phase in higher-melting lipids. It is not a simple matter of increased affinity at higher temperatures, given that αSN passes through the same temperature range in all lipids. Instead the explanation must be found in intrinsic lipid properties.

The lipid-melting transition is characterized by a sharp peak in the heat capacity Δc_p. The heat capacity scales directly with several mechanical properties of the bilayer, which also show a maximum around t_m, including elastic area compressibility (50), the volume expansion coefficient (51), and permeability (52). This maximum is due to the dynamic heterogeneity in this temperature range owing to coexisting domains of gel phase and liquid disordered phase (52). It can be envisaged that the interfacial regions of these domains provide good binding sites for the binding of proteins as well as small nonpolar solutes such as alcohols and fatty acids (53). These properties will also depend on the chain length and t_m. The higher the t_m, the narrower and taller the ΔC_p peak and, in parallel, the compressibility. Yet this chain-length dependent difference in maximum compressibility/permeability only occurs in a narrow temperature range and should not affect lipid properties in regimes outside the transition region. αSN does not have to be heated up in the presence of lipids through the transition region to fold but can insert directly into the fluid disordered phase well above t_m (data not shown). Nevertheless, the phenomenon leads to a linear relationship between the proportion of folded αSN and the lipid-melting temperature, and thus provides an empirical explanation for DOPG's low ability to induce structure in αSN, namely its low t_m (−20°C).

The dependence on vesicle size

It is intriguing that the induction of structure requires vesicles above a certain size. In other words, if the curvature increases beyond a certain threshold, no significant binding occurs. The reliance on large rather than small vesicles runs counter to many of the other examples of curvature-sensitive proteins (35,54–56), which show a lesser degree of folding, activity, or binding when exposed to larger vesicle sizes. In these latter cases, it is thought that cracks or defects in the vesicle surface induced by curvature will provide sites for proteins to bind. These defects also make small vesicles inherently unstable. On standing, particularly below the t_m, they tend to coalesce to vesicles which for DPPC are around 70 nm in size (57), but other phosphatidylcholine vesicles have also been measured to be around 140 nm (58), which is also the minimum size required to induce significant amounts of αSN binding (Fig. 1 *D*). To our knowledge, no data exist for phosphatidylglycerol vesicles, but it seems reasonable to assume that they will assume the same size optimum. Interestingly, smaller vesicles show broader thermal transitions and a lower maximal Δc_p than larger vesicles (59). This is similar to the difference between low-melting lipids and high-melting lipids. Also in this case, higher maximal Δc_p values translate into a larger degree of structure for αSN for lipids with higher melting temperatures, although the Δc_p spike is confined to the transition region. We are at present unable to point to any lipid properties that can explain how these empirical observations may affect lipid properties above the transition region. For example, lateral pressure profiles do not place DOPG in a group apart from the other lipids measured in this study (60).

Our data may appear to contradict previous work that indicates binding of αSN to small unilamellar vesicles (SUVs); however, that work is typically carried out at much higher

lipid/protein ratios (250:1 or higher as in (37)) where the number of binding sites is not limited. The low lipid/protein ratios used by us magnifies any differences between affinities for different lipid sizes. It should also be pointed out that we do not exclude formation of some α-helical structure but rather highlight that vesicle size (whose effect on αSN binding has not previously been systematically probed to our knowledge) may influence the extent of this structural formation and its subsequent loss by thermal denaturation. We should also point out that the occasional deviation from size reliance that we observe in our thermal scans may reflect variations in vesicle size homogeneity and structure that can lead to altered vesicle affinity by αSN. It is well known that vesicle preparations can vary in terms of size distribution and stability against coalescence, and such small variations can affect the binding affinity. However, the unmistakable trend in our observations, measured for numerous different lipids, is a clear separation between the effects of small and large vesicles.

Although our data do not provide clear explanations for the size-dependence, various hypotheses can be proposed. A very recent report by Eliezer and co-workers provides strong evidence from pulsed electron spin resonance (ESR) data that αSN forms an extended helix at least 7 nm long in the presence of vesicles (containing 50% anionic lipids and 50% zwitterionic lipids) and bicelles (23). Similar results were obtained by the Langen group using continuous-wave ESR (24). The uninterrupted α-helical stretch makes the protein potentially sensitive to vesicle curvature, nevertheless the structure of αSN could easily be fitted onto the curved surface of a small 30-nm vesicle (24). Intermolecular interactions between individual extended helices could in principle exacerbate the sensitivity to vesicle size; however, such intermolecular contacts were not reported. It should be noted that αSN may form broken or antiparallel helices under very similar conditions according to other recent ESR studies in conjunction with molecular simulations (25,26), making it difficult to make firm conclusions on how this impacts on the size-dependence. Another possibility is that nonhelical structures can be stabilized by packing defects in strongly curved vesicles; note though that such packing defects tend to be most pronounced for very small vesicles (30 nm diameter), well below the ~100-nm threshold we observe. Furthermore, simple energy considerations, such as the need for internal hydrogen bonding in an environment with reduced water accessibility (42), suggest that αSN must adopt some nonrandom coil structure when it binds to the lipid surface. We have no evidence that αSN adopts other types of secondary structure in the presence of lipids on the short time scales of our experiments in this report.

Implications for the biological function of αSN

Our data thus illustrate that αSN vesicle binding is strongly modulated by lipid properties as well as its intrinsic ability to form α-helical structures in an anionic lipid environment. There are numerous quite different optimal αSN binding conditions. Our observations illustrate that αSN prefers the liquid disordered phase of large anionic vesicles, but other reports detail that αSN can also bind to and fold on small zwitterionic vesicles in the gel phase (35). In the presence of lipid rafts, αSN binding requires anionic lipids (preferentially containing a polyunsaturated acyl chain and a phosphatidylserine headgroup) and the coexistence of different domains (19). Although the structure is α-helical in all cases, we cannot exclude that there are subtle changes in the orientation of the protein, e.g., peripheral versus partially inserted versus transmembrane (37).

It is possible that these structural variations and their dependence on vesicle size may have biological significance. It has been suggested that αSN affects the distal pool of synaptic vesicles (6,61). Synaptic vesicles are close to their transition temperature, meaning that binding is optimal, and αSN could modulate the structure of these lipids or simply select those above a certain size by binding to them and chaperoning them to the cell membrane. αSN may have a negative regulatory role in neurotransmission (62), by e.g., inhibiting docking of synaptic vesicles at active zones of SNARE complexes, possibly by stabilizing them at a size that prevents fusion with SNARE complexes (63,64). This role is confirmed by the observation in yeast that mutants impaired in vesicular trafficking were more sensitive to αSN expression (7), and conversely overexpression of proteins participating in vesicular transport between the ER and Golgi could suppress αSN toxicity (8). The αSN defect probably occurs at the stage of vesicle tethering/docking/fusion at the Golgi (8), in accordance with the pivotal role of αSN-vesicle interactions.

T.H. and D.E.O. are supported by the Villum Kann Rasmussen Foundation through the BioNET research network. We thank Ole G. Mouritsen for discussions and Lars Sottrup-Jensen for generous access to equipment.

REFERENCES

1. Lashuel, H. A., B. M. Petre, J. Wall, M. Simon, R. J. Nowak, et al. 2002. alpha -synuclein, especially the Parkinson's Disease-associated mutants, forms pore-like annular and tubular protofibrils. *J. Mol. Biol.* 322:1089–1102.
2. Volles, M. J., S. -J. Lee, J. -C. Rochet, M. D. Shtilerman, T. T. Ding, et al. 2001. Vesicle permeabilization by protofibrillar α-synuclein: Implications for the pathogenesis and treatment of Parkinson's Disease. *Biochemistry.* 40:7812–7819.
3. Volles, M. J., and P. T. Lansbury. 2002. Vesicle permeabilization by protofibrillar α-synuclein is sensitive to Parkinson's disease-linked mutations and occurs by a pore-like mechanism. *Biochemistry.* 41:4595–4602.
4. Volles, M. J., and P. T. Lansbury. 2003. Zeroing in on the pathogenic form of alpha-synuclein and its mechanism of neurotoxicity in Parkinson's Disease. *Biochemistry.* 42:7871–7878.
5. Danzer, K. M., D. Haasen, A. R. Karow, S. Moussaud, M. Habeck, et al. 2007. Different species of a-synuclein oligomers induce calcium influx and seeding. *J. Neurosci.* 27:9220–9232.

6. Cabin, D. E., K. Shimazu, D. Murphy, N. B. Cole, W. Gottschalk, et al. 2002. Synaptic vesicle depletion correlates with attenuated synaptic responses to prolonged repetitive stimulation in mice lacking alpha-synuclein. *J. Neurosci.* 22:8787–8807.
7. Willingham, S., T. F. Outerio, M. J. DeVit, S. L. Lindquist, and P. J. Muchowski. 2003. Yeast genes that enhance the toxicity of a mutant Huntingtin fragment or α-synuclein. *Science.* 302:1769–1772.
8. Cooper, A. A., A. D. Gitler, A. Cashikar, C. M. Haynes, K. J. Hill, et al. 2006. alpha-synuclein blocks ER-Golgi traffic and Rab1 rescues neuron loss in Parkinson's models. *Science.* 313:234–238.
9. Zhu, M., and A. L. Fink. 2003. Lipid binding inhibits alpha-synuclein fibril formation. *J. Biol. Chem.* 278:16873–16877.
10. Jensen, P. H., M. S. Nielsen, R. Jakes, C. G. Dotti, and M. Goedert. 1998. Binding of alpha-synuclein to brain vesicles is abolished by familial Parkinson's disease mutation. *J. Biol. Chem.* 273: 26292–26294.
11. Perrin, R. J., W. S. Woods, D. F. Clayton, and J. M. George. 2000. Interaction of human alpha-Synuclein and Parkinson's disease variants with phospholipids. Structural analysis using site-directed mutagenesis. *J. Biol. Chem.* 275:34393–34398.
12. Bussell, R., and D. Eliezer. 2004. Effects of Parkinson's disease-linked mutations on the structure of lipid-associated alpha-synuclein. *Biochemistry.* 43:4810–4818.
13. Stöckl, M., P. Fischer, E. Wanker, and A. Herrmann. 2008. Alpha-synuclein selectively binds to anionic phospholipids embedded in liquid-disordered domains. *J. Mol. Biol.* 375:1394–1404.
14. Bussell, R., and D. Eliezer. 2001. Residual structure and dynamics in Parkinson's disease-associated mutants of alpha-synuclein. *J. Biol. Chem.* 276:45996–46003.
15. Chandra, S., G. Gallardo, R. Fernández-Chacon, O. M. Schlüter, and T. C. Südhof. 2005. α-synuclein cooperates with CSP-α in preventing neurodegeneration. *Cell.* 123:383–396.
16. Kim, Y. S., E. Laurine, W. Woods, and S.-J. Lee. 2006. A novel mechanism of interaction between α-synuclein and biological membranes. *J. Mol. Biol.* 360:386–397.
17. Bertoncini, C. W., Y.-S. Jung, C. O. Fernandez, W. Hoyer, C. Griesinger, et al. 2005. Release of long-range tertiary interactions potentiates aggregation of natively unstructured α-synuclein. *Proc. Natl. Acad. Sci. USA.* 102:1430–1435.
18. Ulmer, T. S., A. Bax, N. B. Cole, and R. L. Nussbaum. 2005. Structure and dynamics of micelle-bound human alpha-synuclein. *J. Biol. Chem.* 280:9595–9603.
19. Kubo, S.-I., V. M. Nemani, R. J. Chalkley, M. D. Anthony, N. Hattori, et al. 2005. A combinatorial code for the interaction of α-synuclein with membranes. *J. Biol. Chem.* 280:31664–31672.
20. Zhu, M., J. Li, and A. L. Fink. 2003. The association of alpha-synuclein with membranes affects bilayer structure, stability and fibril formation. *J. Biol. Chem.* 278:40186–40197.
21. Jo, E., J. McLaurin, C. M. Yip, P. St. George-Hyslop, and P. E. Faser. 2000. alpha-synuclein membrane interactions and lipid specificity. *J. Biol. Chem.* 275:34328–34334.
22. Broersen, K., D. van den Brink, G. Fraser, M. Goedert, and B. Davletov. 2006. Alpha-synuclein adopts an alpha-helical conformation in the presence of polyunsaturated fatty acids to hinder micelle formation. *Biochemistry.* 45:15610–15616.
23. Georgieva, E. R., T. F. Ramlall, P. P. Borbat, J. H. Freed, and D. Eliezer. 2008. Membrane-bound alpha-synuclein forms an extended helix: long-distance pulsed ESR measurements using vesicles, bicelles, and rodlike micelles. *J. Am. Chem. Soc.* 130:12856–12857.
24. Jao, C. C., B. G. Hegde, J. Chen, I. S. Haworth, and R. Langen. 2008. Structure of membrane-bound alpha-synuclein from site-directed spin labeling and computational refinement. *Proc. Natl. Acad. Sci. USA.* 105:19666–19671.
25. Drescher, M., G. Veldhuis, B. D. van Rooijen, S. Milikisyants, V. Subramaniam, et al. 2008. Antiparallel arrangement of the helices of vesicle-bound alpha-synuclein. *J. Am. Chem. Soc.* 130:7796–7797.
26. Bortolus, M., F. Tombolato, I. Tessari, M. Bisaglia, S. Mammi, et al. 2008. Broken helix in vesicle and micelle-bound alpha-synuclein: insights from site-directed spin labeling-EPR experiments and MD simulations. *J. Am. Chem. Soc.* 130:6690–6691.
27. Sharon, R., M. S. Goldberg, I. Bar-Josef, R. A. Betensky, J. Shen, et al. 2001. alpha-Synuclein occurs in lipid-rich high molecular weight complexes, binds fatty acids, and shows homology to the fatty acid-binding proteins. *Proc. Natl. Acad. Sci. USA.* 98:9110–9115.
28. Sharon, R., I. Bar-Joseph, M. P. Frosch, D. M. Walsh, J. A. Hamilton, et al. 2003. The formation of highly soluble oligomers of alpha-synuclein is regulated by fatty acids and enhanced in Parkinson's disease. *Neuron.* 37:583–595.
29. Davidson, W. S., A. Jonas, D. F. Clayton, and J. M. George. 1998. Stabilization of alpha-synuclein secondary structure upon binding to synthetic membranes. *J. Biol. Chem.* 273:9443–9449.
30. Ramakrishnan, M., P. H. Jensen, and D. Marsh. 2003. Alpha-synuclein association with phosphatidylglycerol probed by lipid spin label. *Biochemistry.* 42:12919–12926.
31. Madine, J., J. Hughes, A. J. Doig, and D. A. Middleton. 2008. The effects of alpha-synuclein on phospholipid vesicle integrity: a study using 31P NMR and electron microscopy. *Mol. Membr. Biol.* 25:518–527.
32. Giannakis, E., J. Pacifico, D. P. Smith, L. W. Hung, C. L. Masters, et al. 2008. Dimeric structures of alpha-synuclein bind preferentially to lipid membranes. *Biochim. Biophys. Acta.* 1778:1112–1119.
33. Bussell, R., T. F. Ramlall, and D. Eliezer. 2005. Helix periodicity, topology, and dynamics of membrane-associated alpha-synuclein. *Protein Sci.* 14:862–872.
34. Bisaglia, M., I. Tessari, L. Pinato, M. Bellanda, S. Giraudo, et al. 2005. A topological model of the interaction between alpha-synuclein and sodium dodecyl sulfate micelles. *Biochemistry.* 44:329–339.
35. Nuscher, B., F. Kamp, T. Mehnert, S. Odoy, C. Haass, et al. 2004. alpha-synuclein has a high affinity for packing defects in a bilayer membrane: a thermodynamics study. *J. Biol. Chem.* 279:21966–21975.
36. Kamp, F., and K. Beyer. 2005. Binding of α-synuclein affects the lipid packing in bilayers of small vesicles. *J. Biol. Chem.* 281:9251–9259.
37. Zakharov, S. D., J. D. Hulleman, E. A. Dutseva, Y. N. Antonenko, J.-C. R. Ochet, et al. 2007. Helical α-synuclein forms highly conductive ion channels. *Biochemistry.* 46:14369–14379.
38. Lindersson, E., D. Lundvig, C. Petersen, P. Madsen, P. Højrup, et al. 2005. P25a is co-expressed with α-synuclein in α-synucleinopathies and stimulates its aggregation. *J. Biol. Chem.* 280:5703–5715.
39. Wimmer, R., K. Andersen, B. Vad, M. Davidsen, S. Mølgaard, et al. 2006. Versatile interactions of the antimicrobial peptide Novispirin with detergents and lipids. *Biochemistry.* 45:481–497.
40. Schneider, M. F., D. Marsh, W. Jahn, B. Kloesgen, and T. Heimburg. 1999. Network formation of lipid membranes: triggering structural transitions by chain melting. *Proc. Natl. Acad. Sci. USA.* 96:14312–14317.
41. Heimburg, T. 2007. Thermal Biophysics of Membranes Wiley-VCH, Berlin.
42. White, S. H., and W. C. Wimley. 1999. Membrane protein folding and stability: physical principles. *Annu. Rev. Biophys. Biomol. Struct.* 28:319–365.
43. Privalov, P. L. 1990. Cold denaturation of proteins. *Crit. Rev. Biochem. Mol. Biol.* 25:281–305.
44. Heimburg, T., and D. Marsh. 1995. Protein surface-distribution and protein-protein interactions in the binding of peripheral proteins to charged lipid membranes. *Biophys. J.* 68:536–546.
45. Privalov, P. L., and G. I. Makhatadze. 1990. Heat capacity of proteins II. Partial molar heat capacity of the unfolded polypeptide chains of proteins: protein unfolding effects. *J. Mol. Biol.* 213:385–391.
46. Ivanova, V. P., I. Makarov, T. E. Schäffer, and T. Heimburg. 2003. Analyzing heat capacity profiles of peptide-containing membranes: cluster formation of gramicidin A. *Biophys. J.* 84:2427–2439.
47. Zuckermann, M. J., and T. Heimburg. 2001. Insertion and pore formation driven by adsorption of proteins onto lipid bilayer membrane-water interfaces. *Biophys. J.* 81:2458–2472.

48. Heimburg, T., B. Angerstein, and D. Marsh. 1999. Binding of peripheral proteins to mixed lipid membranes: the effect of local demixing upon binding. *Biophys. J.* 76:2575–2586.

49. Cole, N. B., D. D. Murphy, T. Grider, S. Rueter, D. Brasaemle, et al. 2002. Lipid droplet binding and oligomerization properties of the Parkinson's disease protein alpha-synuclein. *J. Biol. Chem.* 277: 6344–6352.

50. Evans, E., and R. Kwok. 1982. Mechanical calorimetry of large dimyristoylphosphatidylcholine vesicles in the phase transition region. *Biochemistry.* 21:4874–4879.

51. Heimburg, T. 1998. Mechanical aspects of membrane thermodynamics. Estimation of the mechanical properties of lipid membranes close to the chain melting transition from calorimetry. *Biochim. Biophys. Acta.* 1415:147–162.

52. Jørgensen, K., J. H. Ipsen, O. G. Mouritsen, and M. J. Zuckermann. 1993. The effect of anaesthetics on the dynamic heterogeneity of lipid membranes. *Chem. Phys. Lipids.* 65:205–216.

53. Westh, P., and C. Trandum. 1999. Thermodynamics of alcohol–lipid bilayer interactions: application of a binding model. *Biochim. Biophys. Acta.* 1421:261–272.

54. Peter, B. J., H. M. Kent, I. G. Mills, Y. Vallis, P. J. Butler, et al. 2003. BAR domains as sensors of membrane curvature: the amphiphysin BAR structure. *Science.* 303:495–499.

55. Huang, H., J. M. Ball, J. T. Billheimer, and F. Schroeder. 1999. Interaction of the N-terminus of sterol carrier protein 2 with membranes: role of membrane curvature. *Biochem. J.* 344 Pt 2:593–603.

56. Shi, J., C. W. Heegaard, J. T. Rasmussen, and G. E. Gilbert. 2004. Lactadherin binds selectively to membranes containing phosphatidyl-L-serine and increased curvature. *Biochim. Biophys. Acta.* 1667:82–90.

57. Schullery, S. E., C. F. Schmidt, P. Felgner, T. W. Tillack, and T. E. Thompson. 1980. Fusion of dipalmitoylphosphatidylcholine vesicles. *Biochemistry.* 19:3919–3923.

58. Ivanova, V. P. 2000. Theoretical and experimental study of protein-lipid interactions. University of Göttingen.

59. Ivanova, V. P., and T. Heimburg. 2001. A histogram method to obtain heat capacities in lipid monolayers, curved bilayers and membranes containing peptides. *Phys. Rev. E Stat. Nonlin. Soft Matter Phys.* 63:1914–1925.

60. Cantor, R. S. 1999. Lipid composition and the lateral pressure profile in bilayers. *Biophys. J.* 76:2625–2639.

61. Murphy, D. D., S. M. Rueter, J. Q. Trojanowski, and V. M. Lee. 2000. Synucleins are developmentally expressed, and alpha-synuclein regulates the size of the presynaptic vesicular pool in primary hippocampal neurons. *J. Neurosci.* 20:3214–3220.

62. Abeliovich, A., Y. Schmitz, D. Farinas, W. H. Choi-Lundberg, C. P. E. Ho, et al. 2000. Mice lacking alpha-synuclein display functional deficits in the nigrostriatal dopamine system. *Neuron.* 25:239–252.

63. Cooper, A. 2008. Neurodegeneration and protein misfolding - What's gone wrong with the cell? *Australian Biochemist.* 39:15–20.

64. Wojcik, S. M., and N. Brose. 2007. Regulation of membrane fusion in synaptic excitation-secretion coupling: speed and accuracy matter. *Neuron.* 55:11–24.